

Retrapping current, self-heating, and hysteretic current-voltage characteristics in ultranarrow superconducting aluminum nanowires

Peng Li, Phillip M. Wu, Yuriy Bomze, Ivan V. Borzenets, Gleb Finkelstein, and A. M. Chang*

Department of Physics, Duke University, Durham, North Carolina 27708, USA

(Received 20 June 2011; published 8 November 2011)

Hysteretic I - V (current-voltage) curves are studied in narrow Al nanowires. The nanowires have a cross section as small as 50 nm^2 . We focus on the retrapping current in a down-sweep of the current, at which a nanowire re-enters the superconducting state from a normal state. The retrapping current is found to be significantly smaller than the switching current at which the nanowire switches into the normal state from a superconducting state during a current up-sweep. For wires of different lengths, we analyze the heat removal due to various processes, including electron and phonon processes. For a short wire $1.5 \mu\text{m}$ in length, electronic thermal conduction is effective; for longer wires $10 \mu\text{m}$ in length, phonon conduction becomes important. We demonstrate that the measured retrapping current as a function of temperature can be quantitatively accounted for by the self-heating occurring in the normal portions of the nanowires to better than 20% accuracy. For the phonon processes, the extracted thermal conduction parameters support the notion of a reduced phase-space below three dimensions, consistent with the phonon thermal wavelength having exceeded the lateral dimensions at temperatures below $\sim 1.3 \text{ K}$. Nevertheless, surprisingly the best fit was achieved with a functional form corresponding to three-dimensional phonons, albeit requiring parameters far exceeding known values in the literature.

DOI: [10.1103/PhysRevB.84.184508](https://doi.org/10.1103/PhysRevB.84.184508)

PACS number(s): 74.25.Sv, 74.78.Na, 74.25.F-, 73.23.-b

Understanding the dynamics of ultranarrow superconducting (SC) nanowire wires is an active area of investigation.¹⁻¹⁵ A significant area of focus is the so-called one-dimensional (1D) limit, delineated by the condition $(w, h) < \xi$, where w is the width and h the height of the nanowire, and ξ is the superconducting coherence length. Investigations of the behavior under current biasing not only elucidate the conditions and limitations for the current carrying capabilities, as well as the process of recovery back into the superconducting (SC) state after driven normal by an excessive current, but also potentially lay the foundation and pave the way for the development of novel devices, such as a current-Josephson effect devices¹⁶ or qubits.¹⁷

In this work we report on measurements carried out in ultranarrow Al nanowires with a cross section as small as 50 nm^2 . The three nanowires studied have widths and heights ranging between 7 and 10 nm, and lengths of $1.5 \mu\text{m}$ (wire S1) or $10 \mu\text{m}$ (wires S2 and S4). These nanowires are exceedingly uniform in their cross section, as indicated by their ability to carry sizable current before being driven normal, where the current density is nearly identical to coevaporated 2D films. In a previous work, the behavior of the switching current I_s during an up-sweep of the current was investigated.⁸ There it was found that heat deposited by phase-slips—transient temporal-spatial events during which the superconducting phase fluctuates and changes by 2π over a distance of order ξ , while the core region goes normal—leads to a thermal runaway, driving the entire nanowire into a normal state from the SC state.

Here we focus on the down-sweep retrapping current. The retrapping current I_r is found to be significantly smaller than the up-sweep switching current I_s , and can be as much as a factor of 20 smaller. The history dependent current-voltage (I - V) relation exemplified by the disparate behaviors in the up- and down-sweep is ubiquitous, despite the fact that based on the criteria normally applied to SNS (superconductor-normal metal-superconductor) bridges, the nanowires should be in the

heavily overdamped regime in its dynamics.^{6,7,18} In MoGe nanowires of widths $\sim 10 \text{ nm}$, Tinkham *et al.*⁶ performed a heat flow analysis, and ascribed the retrapping behavior to self-heating. Our work bears similarity to that work, but our SC nanowires are in a different regime, where $k_F l \sim 60 \gg 1$, rather than being close to 1 in their case. Here k_F is the Fermi wave number and l is the mean-free path. Moreover, their nanowires were suspended freely, while ours are deposited onto a narrow, 8-nm-wide InP ridge [Fig. 1(a)], and are thus in thermal contact with an underlying substrate. Furthermore, our analysis differs from theirs in the form of the heat flow equations. Based on our analysis, we rule out underdamping as the cause of the hysteresis, in agreement with recent results in submicron SNS bridges.¹⁸

To lay the framework for understanding the behavior of nanowires, the Josephson junction can serve as a starting point. There, the free energy landscape under current bias is described by the tilted washboard potential, shown in Fig. 2(a).¹⁹ This same scenario is also applicable to 1D SC nanowires.^{11,12} Josephson junctions are classified within a resistively and capacitively shunted junction (RCSJ) model as either under- or overdamped, depending on whether the quality factor $Q = \sqrt{2eI_c C / \hbar R}$ is greater or less than 1. Here I_c is the critical Josephson current, C is the junction capacitance, and R is the junction normal state resistance. When the underdamped Josephson junction is driven over the free-energy barrier out of its metastable minimum, the SC phase keeps running downhill as there is insufficient damping to retrap the phase in a lower energy local minimum. A consequence is a hysteretic current-voltage (I - V) relation, where the up-sweep and down-sweep branches do not overlap. In contrast, in an overdamped junction, the phase moves diffusively between adjacent minima, and hysteresis is often not present.²¹⁻²³

The estimated Q for our nanowires is in the range of ~ 0.01 , far below unity, and the nanowires are ostensibly in the severely overdamped limit. This estimate is relevant when the nanowire

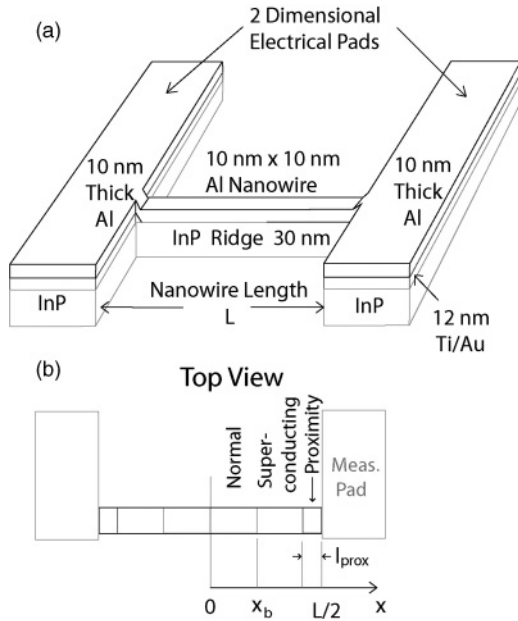


FIG. 1. (a) Schematic of the Al superconducting nanowire device on a narrow InP ridge template. The ends of the nanowire are connected to large, electrical measurement pads. The pads can either be in the superconducting state or driven normal by a magnetic field. (b) Top view of the nanowire geometry, and the layout used in the heat flow model discussed in the text.

device is in the S-NW-S configuration, where S refers to each of the two large metallic measurement pads when in the SC state, and NW denotes the nanowire. It also provides a reasonable estimate in the N-NW-N configuration, when the pads are driven normal, but the ambient temperature is below the nanowire SC transition temperature T_c . In this case, the nanowire itself breaks up into alternating SC and normal segments, whether during an up-sweep or a down-sweep of the current. In the former case, the nanowire is overall in the SC state, but during a phase-slip, the phase-slip normal core acts as the normal region. In the latter, the central portion of the nanowire is normal due to heating, while the regions closer to the pads are in the SC state [Fig. 1(b)].

Nevertheless, despite the overdamping, hysteretic I - V curves are ubiquitous, as can be seen for wire S2 in Fig. 2. In fact, the ratio of I_r to I_s can be as small as $\sim 1/20$. For example, in nanowire S2 at $T \sim 0.3$ K, $I_r \sim 0.19$ μ A, while $I_s \sim 4$ μ A. These observations motivated us to investigate the retrapping current systematically as a function of the temperature and wire length, and to perform a detailed heat analysis to establish self-heating as a cause of the substantially reduced I_r below the value of the up-sweep I_s .

Our devices were fabricated using a template method. The template is a narrow, 8-nm-wide InP ridge, formed by differential etching on the cleaved (110) crystallographic plane of a molecular-beam-epitaxy (MBE) grown InGaAs-InP crystal, where the growth direction is (001). The geometry of our devices is depicted in Fig. 1(a). The details of the fabrication procedure is described in a previous work.²⁴ The nanowire resides on the narrow InP ridge and is thus thermally connected to the large semiconductor substrate through the narrow ridge. The nanowire is electrically connected to large

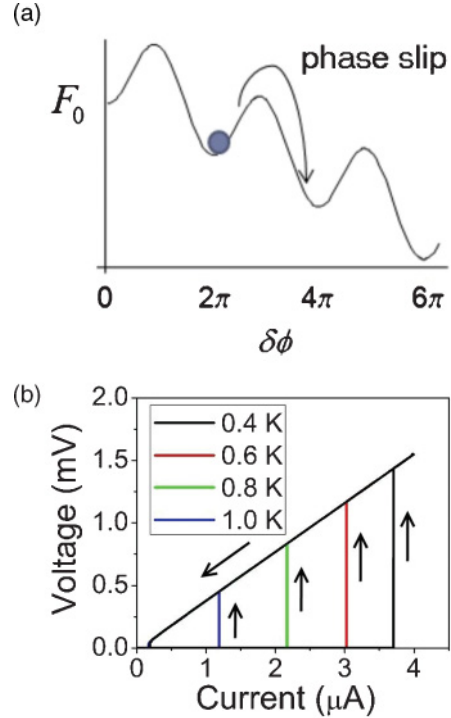


FIG. 2. (Color online) (a) Tilted-washboard free energy landscape for a Josephson junction under current bias. A phase slip occurring between adjacent minima is indicated. A similar scenario occurs in a 1D superconducting nanowire. (b) Hysteretic I - V curves for nanowire S2 at several temperatures. Arrows indicate direction of current sweeps. The up-sweep switching current I_s is significantly larger than the down-sweep retrapping current I_r .

metallic measurement pads on its ends. Therefore, for heat removal, thermal conduction both in the lateral direction along the nanowire, and vertically through the InP ridge via phonon processes must be considered. The I - V measurements were carried out in a shielded copper can to minimize unwanted environmental interference, such as external noise (e.g., from nearby radio stations) conducted down the electrical cables, or Johnson-Nyquist noise from resistors within the electrical measurement circuitry. In particular, Thermocoax cables with the ability to remove high-frequency noise is employed where possible, as well as low-temperature rf filters. The devices are also enclosed in metal cans with all openings plugged with conductive tape or metal mesh.

In Figs. 3(a)–3(c) we present the measured I_r for the three nanowires S1 ($10 \text{ nm} \times 10 \text{ nm} \times 1.5 \text{ }\mu\text{m}$), S2 ($9.3 \text{ nm} \times 9.3 \text{ nm} \times 10 \text{ }\mu\text{m}$), and S4 ($7 \text{ nm} \times 7 \text{ nm} \times 10 \text{ }\mu\text{m}$), respectively, as a function of temperature. Immediately apparent is the substantial difference in the magnitude of the retrapping current I_r for the short S1, when compared to the longer S2 and S4. For S1, $I_r = 0.99$ μ A at $T = 0.3$ K, while it is 0.19 and 0.117 μ A, respectively for S2 and S4. Thus, the value of I_r in S1 is roughly 5–8 times that in S2 or S4. The results for S2 and S4 do not depend on whether measurements were carried out in the S-NW-S or the N-NW-N configuration. In contrast, for S1, due to the larger current level and associated excessive heating, it was necessary to drive the measurement pads into a normal state, into the N-NW-N configuration. By driving these pads into

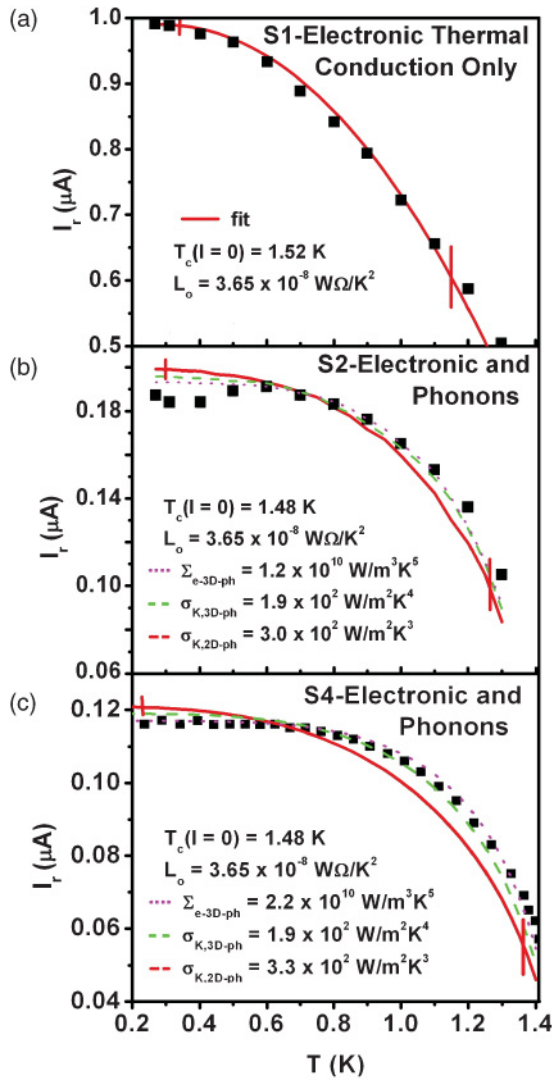


FIG. 3. (Color online) Solid squares: Data for the retrapping current I_r as a function of temperature for nanowires. (a) S1 ($10 \text{ nm} \times 10 \text{ nm} \times 1.5 \text{ } \mu\text{m}$), (b) S2 ($9.3 \text{ nm} \times 9.3 \text{ nm} \times 10 \text{ } \mu\text{m}$), and (c) S4 ($7 \text{ nm} \times 7 \text{ nm} \times 10 \text{ } \mu\text{m}$). For S1 in (a), the solid curve is a fit based on the heat flow model described in the main text, where only the electronic thermal conduction is considered. The Wiedermann-Franz constant deduced from the fitting is $L_o = 3.65 \pm 0.15 \times 10^{-8} \text{ W}\Omega/\text{K}^2$. Vertical bars indicate certainty of the fitting curve due to a combination of the uncertain in the parameters, including uncertain in the superconducting transition temperature $T_c(I)$ of $\pm 2\%$. For S2 and S4 it is necessary to include both electronic and phonon conduction. Various rate limiting phonon processes were considered, including electron phonon relaxation and Kapitza boundary resistance phonon conduction (see text). The uncertain of the phonon parameters is $\pm 10\%$.

the normal state using a small magnetic field $B = 0.1 \text{ T}$, the now normal pads can act as good thermal anchors, keeping the temperatures of the ends at the ambient temperature T_o . For the longer S2 and S4, the smaller current level means that a much lower amount of heat needs to be carried out through wire ends; thus improved thermal anchoring was not needed. For S1, on the other hand, keeping the pads

SC (S-NW-S configuration) reduced I_r to $\sim 0.55 \text{ } \mu\text{A}$ from $\sim 1 \text{ } \mu\text{A}$ as heat removal becomes more difficult due to poor thermal conduction capability of the SC pads. At the same time, instabilities arise in the temperature profile along the nanowire, leading to very noisy data below 0.8 K with I_r fluctuating as much as $0.1 \text{ } \mu\text{A}$ between adjacent data points.

The 0.1 T magnetic field affects the nanowires and the large, two-dimensional electrical pads differently. The nanowires are able to keep SC at low current levels with an overall behavior similar to their zero magnetic field behavior, while the pads are driven into the normal state. This difference occurs because the nanowires and the pads behave as type II superconductors, similar to most thin film superconductors. In the pads, the upper critical field H_{c2} is set by the condition of having roughly on flux quantum ($h/2e$) fit in the area A of a square with sides ξ the (superconducting) coherence length, that is, $A \sim \xi^2$. In the nanowires, since the width w is much smaller than ξ , the area A is now given by ξw , resulting in an enhanced H_{c2} above its value for the pads by a factor ξ/w . Typically, for the nanowires H_{c2} ranges from 0.5 to 2 T between 20 mK and 1.4 K , while for the pads it is below 0.05 T at all temperatures.

The configuration with *normal* electrical pads is relevant for our data in Fig. 3. *In the analysis which follows, we will focus on this configuration.* The retrapping process returns a nanowire into the SC state during a down-sweep of the current I at an ambient lattice temperature T_o below the zero current critical temperature $T_c(I = 0)$. At large I , most of the nanowire remains normal due to self-heating, which raises the local temperature above the switching temperature at that current $T_s(I)$.

During a current down-sweep, the temperature is position dependent along the nanowire. In the N-NW-N configuration, each of its ends is connected to a large, normal metal electrical measurement pads, anchored at T_o . Because $T_o < T_c(I = 0)$, and is in fact below $T_s(I = I_r)$, the end regions are in the SC state, aside from a short proximity region $l_{\text{prox}} \sim 100 \text{ nm}$ in length, immediately adjacent to each normal pad [Fig. 1(b)]. Here the $T_s(I)$ is the up-sweep switching temperature at current I . On the other hand, as long as I exceeded I_r , the center of the nanowire is above $T_s(I)$ and is thus in the normal state. When I is reduced down to I_r , a blockage preventing the central region to be cooled is suddenly removed, allowing the cooling to propagate all the way to the center. This blockage removal is described in detail in what follows.

The up-sweep switching temperature for a given current $T_s(I)$ expresses the same relation as the switch current as a function of temperature $I_s(T)$, but viewed in reverse. For our nanowires, these were reported in Ref. 8. It is worthwhile to point out that the value of I_s at a given temperature is not unique, but depends on the up-sweep ramp rate of the current. Conversely, $T_s(I)$ is also dependent on the ramp rate. This is due to the fact that the switching is caused by phase-slip events,⁷⁻⁹ and thus the relative rates of the phase-slip generation to current up-sweep matters. The slower the up-sweep current ramp rate, the longer waiting time is available for phase-slip events to take place within a given interval in current. This increases the probability for switching within that interval and reduces the magnitude of the current at which switching takes place. But because the rate of phase-slip generation is exponentially dependent on the current, the

dependence of I_s on ramp rate is weak, and is approximately logarithmic.

To estimate I_r , it is necessary to determine the position dependent temperature $T(x)$. Both the electronic and phonon thermal conduction mechanisms need to be considered. The temperature range of interest is very low compared to the lattice Debye temperature $\Theta_D \sim 300$ K and the temperature dependence of the phonon thermal conductivity takes a power-law form, reflecting the phonon density of states. At these low temperatures, $0.2 < T < 1.3$ K, the value of the phonon conductivity is considerably smaller than the electronic thermal conductivity. The only exception is in the SC regions when $T(x) < 0.35$ K. Thus, in the absence of a very large temperature rise phonons can only carry away a relatively small amount of heat. Whereas electronic conduction requires the heat to exit the ends of the nanowire, the phonon conduction goes through the short InP template ridge (in height), on which the nanowire resides. The nanowire length is microns while the ridge is only 30 nm in height. If the wire is long, the electronic mechanism will become much less effective, and phonon conduction must be included as well.

For the short wire S1, electronic conduction overwhelmingly dominates. For the long wire S2, both electronic and phonon thermal conduction must take place side by side. Phonon conduction through the InP ridge takes place via several steps: (a) electron-phonon energy relaxation within the aluminum nanowire, (b) conduction through the aluminum-InP boundary, and (c) conduction through the 8-nm-wide, 30-nm-tall InP ridge. Below the ridge, the energy is dissipated in the very highly conductive GaAs bulk material. Thus the base of the InP ridge can safely be assumed to be held at the ambient temperature T_o .

One additional mechanism of heat removal takes place through the liquid He^3 , which surrounded the nanowires in the set of measurement on S1 and S2. However, this channel appears less important. Additional data for wire S4 obtained in the dilution refrigerator, in which the samples are in vacuum and thus there was no liquid surrounding the nanowire, yielded a retrapping current which can be accounted for in a similar manner as S2, using electronic and InP ridge thermal conduction only. Note both wires S2 and S4 are $10 \mu\text{m}$ in length.

We divide a nanowire into two symmetric halves of length $L/2$ each, where L is the total wire length, and consider the right half, where $0 \leq x \leq L/2$, and $T(x = L/2) = T_o$, as shown in Fig. 1(b). When slowly down-sweeping the current I , we assume that the nanowire is in the SC state at a position x , if $T(x) < T_s(I)$, but is in a normal state if $T(x) > T_s(I)$.

We begin by considering the short wire S1 ($1.5 \mu\text{m}$ in length) and only include electronic conduction. Phonon conduction alone will remove $\sim 3\%$ of the heat generated by heating, and will be neglected. The diffusion equations must account for three regions: (a) the central region for $0 \leq x \leq x_b$, which is normal for $I > I_r$ and has a resistance per unit length of $R_N/L \sim 0.33 - 0.82 \text{ k}\Omega/\mu\text{m}$ (Ref. 8) and thus self-heats; (b) the SC segment for $x_b \leq x \leq L/2 - l_{\text{prox}}$, which nearly does not self-heat, but must conduct the heat generated by the central normal segment, and (c) the short proximity region adjacent to the normal metal pads for $L/2 - l_{\text{prox}} \leq x \leq L/2$ which is approximated as a normal region. More precisely, the

SC region close to the SC-normal boundary x_b heats slightly due to occasional phase slips as its temperature is just below $T_s(I) \geq 1.1$ K; the proximity region generates self-heating, and in addition must conduct through it the heat of the central normal region as well. For the normal metal regions, the steady state heat diffusion equation is given by

$$\frac{I^2 R_N}{L} = -\frac{d}{dx} \left(\kappa_N A_{\text{nw}} \frac{dT}{dx} \right), \quad (1)$$

where $\kappa_N = L_o L T / (R_N A_{\text{nw}})$ is the electronic Wiedemann-Franz electronic thermal conductivity, L_o is Lorenz number determined from fitting, and $A_{\text{nw}} = w \times h$ the nanowire cross sectional area. In the SC region, it is replaced by

$$0 \approx -\frac{d}{dx} \left(\kappa_{\text{SC}} A_{\text{nw}} \frac{dT}{dx} \right). \quad (2)$$

The equations in the three regions are supplemented by boundary conditions at the junctions. The junction between the center normal region and the SC region takes place at $x = x_b$, and between the SC and short proximity regions at $x = L/2 - l_{\text{prox}}$. The temperature is continuous across each junction, and the heat flow is identical immediately to the left and right. Finally, we have $T(x = L/2) = T_o$. Note that the forms of these equations differ from those used in Ref. 6. There the variation of the thermal conductivity κ_N or κ_{SC} with position, through their dependence on temperature T , was not accounted for.⁶

At a given temperature below $T_c(I)$, the electronic thermal conductivity of the SC segment at a position x , with a temperature $T(x)$, is related to the corresponding normal metal W-F thermal conductivity at that temperature, by the ratio $r \equiv \kappa_{\text{SC}}/\kappa_N$:¹⁸

$$r = \frac{3}{\pi^2} \int_{1.76T_c(I)/T(x)}^{\infty} \frac{y^2}{\cosh^2(y/2)} dy. \quad (3)$$

This integral evaluated numerically is shown in Fig. 4. For the purpose of determining the position dependent temperature at a given I , this ratio is approximated by a linear form as indicated in the figure for $0.2 < T(x)/T_c(I) < 1$:

$$r \approx 1.125[T(x)/T_c(I) - 0.2]. \quad (4)$$

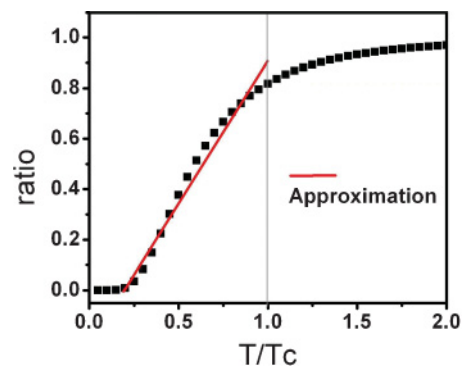


FIG. 4. (Color online) Plot of the thermal heat capacity ratio $\kappa_{\text{SC}}/\kappa_N$ between the normal and superconducting states, as a function of reduced temperature T/T_c . The line indicates the approximation used in the calculations.

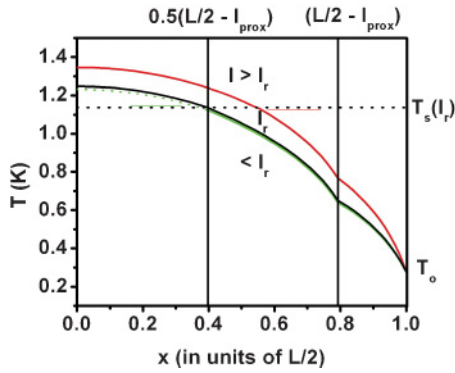


FIG. 5. (Color online) The temperature profile vs position x at ambient temperature T_0 , with a corresponding retrap current I_r . Three different current levels are depicted: $I > I_r$, $I = I_r$, and $I < I_r$. The critical value of the SC-normal boundary is given approximately by $x_c = 0.5(L/2 - l_{\text{prox}})$. The proximity region lies to the right of $x = (L/2 - l_{\text{prox}})$, ending at the electrical pad at $L/2$. The SC segment lies immediately to the left. For $I \geq I_r$, the position of the SC-normal boundary x_b is given by the intersection of $T(x)$ and the corresponding switching current $T_s(I)$. The horizontal dotted line depicts $T_s(I_r)$, while the short light solid lines correspond to $I < I_r$ and $I > I_r$ with $[T_s(I > I_r)] < [T_s(I_r)] < [T_s(I < I_r)]$. For $I > I_r$, $x_b > x_c$. For $I = I_r$, $x_b = x_c$. For $I < I_r$, indicated by the light solid curve joined onto the light dotted curve, the dotted “normal” region is unstable; the region immediately to the left of x_c actually falls below $T_s(I < I_r)$ and will go superconducting, leading to a propagation of the SC-normal boundary toward the center at $x = 0$.

We next describe how the cooling blockage can be removed, and determine the condition for this to occur. To do so we consider the SC region and fix the current at I . The SC-normal boundary occurs at x_b , which is determined by equating the temperature at x_b , $T(x_b)$, to the switching temperature at that current $T_s(I)$. Momentarily treating x_b as a variable, $T(x_b)$ attains its maximum value at a critical value $x_b = x_c$; in the simplest approximation x_c is independent of I as will be seen below. For a large current I , the normal region is large and the actual x_b exceeds x_c (Fig. 5). As I is reduced down to I_r , the normal region shrinks and x_b becomes equal to x_c . Here $T(x_b = x_c)$ takes on the maximum possible value at I_r , since $x_b = x_c$, and is equal to $T_s(I_r)$. Further reducing I to just below I_r , $T_s(I < I_r)$ will slightly increase from $T_s(I_r)$, while at every x , $T(x)$ will slightly decrease due to reduced heating. The decreased maximum temperature at x_c , $T(x = x_c)$, can no longer reach the increased $T_s(I < I_r)$. The boundary will become unstable, and will propagate toward the center at $x = 0$. Starting from the initial boundary at $x_b = x_c$, more and more of the normal region will fall below $T_s(I)$ and become superconducting, as the shrinking normal region generates less and less heat, until the entire wire is cooled. The three cases are depicted in Fig. 5.

The value for x_c can be deduced from the steady-state heat diffusion equation in the SC state [Eq. (2)]. Neglecting the short proximity region adjacent to the pad, $x_c = L/4 [0.5(L/2)]$; accounting for the proximity region of length l_{prox} modifies this to $x_c \approx (L/2 - l_{\text{prox}})/2$. For illustrative purposes, let us determine x_c in the absence of the proximity region. Focusing on the SC region at its border with the normal

segment $x = x_b$, twice integrating the diffusion equation and matching the boundary conditions yields for the left-hand-side (LHS)

$$\text{LHS} = \left(I^2 R_N \frac{x}{L} \right) (L/2 - x), \quad (5)$$

which is maximal for $x = L/4$ for fixed I . At $x = x_b$ the factor $I^2 R_N \frac{x}{L}$ represents the heating power generated by the normal region where $0 \leq x \leq x_b$. Equating the LHS to a twice-integrated right-hand side and solving for $T(x_b)$ thus yields the highest temperature at the normal-SC border when $x_b = x_c = L/4$, where the LHS is maximal.

Using the approximate form of the thermal conductivity ratio r between the SC and normal states given by Eq. (4), the diffusion equation can readily be solved analytically. The solution yielded the position dependent temperature profile shown in Fig. 6(a). The kink at the SC-proximity boundary is an artifact of our model, where the proximity region is approximated as a normal region. A more accurate model would require solving the Usadel equation, which is expected

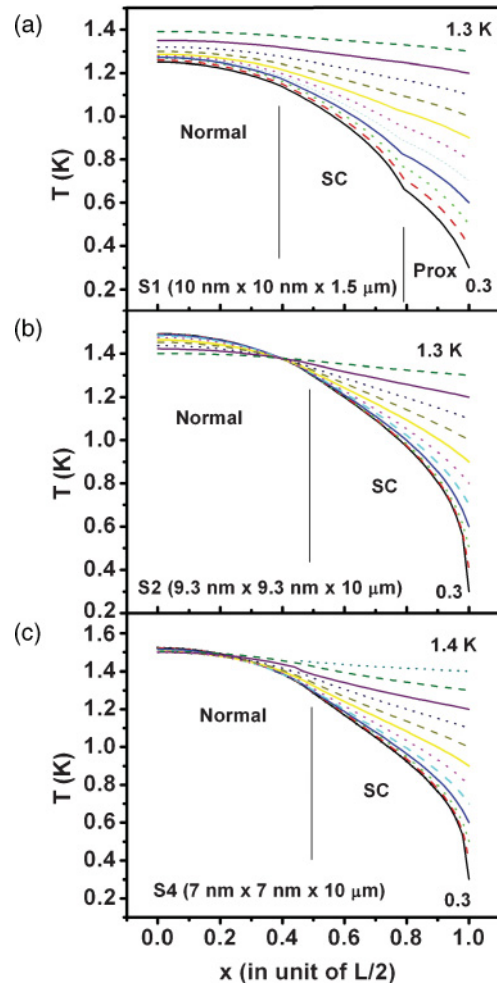


FIG. 6. (Color online) Temperature profile vs position x for different ambient temperatures. The temperature is stepped by 0.1 K between successive curves—(a) nanowire S1, (b) nanowire S2, and (c) nanowire S4. The kink at $x = 0.79(L/2)$ in (a) is an artifact of modeling the proximity region as a normal metal, with a sharp boundary with the SC region to its left.

to yield a rounding and smoothing of the kink. See Ref. 24 for an example of the rounded voltage profile in the proximity region. The fit to the I_r as a function of temperature T is presented in Fig. 3(a) using a Lorenz number $L_o = 3.65 \times 10^{-8} \text{ W } \Omega/\text{K}^2$, somewhat higher than the theoretical value of $2.45 \times 10^{-8} \text{ W } \Omega/\text{K}^2$. Viewed in another way, forcing L_o to take the theoretical value, our model would predict a low temperature $I_r \sim 0.8 \mu\text{A}$, rather than the $1 \mu\text{A}$ we observed. Reconciling this discrepancy may require the development of more sophisticated analysis using the Usadel equation, while incorporating heating and a position dependent temperature at the same time. Despite the discrepancies, the overall behavior and magnitude (within 20% accuracy) are captured in our simple model.

For the $10 \mu\text{m}$ wires S2 and S4, electronic thermal conduction alone is not sufficient to support the measured I_r , despite its smaller value (by a factor of 5–8 at 0.3 K). It is necessary to include phonon conduction. We assume a power-law temperature dependence in the heat exchange rate. At every position, the heat-removal linear power density is set proportional to $T^\gamma - T_o^\gamma$, where γ may be varied to reflect the limiting process in the phonon conduction discussed above. The steady-state heat diffusion equation takes the forms

$$\frac{I^2 R_N}{L} - \beta(T^\gamma - T_o^\gamma) = -\frac{d}{dx} \left(\kappa_N A_{\text{nw}} \frac{dT}{dx} \right) \quad (6)$$

and

$$-\beta(T^\gamma - T_o^\gamma) \approx -\frac{d}{dx} \left(\kappa_{\text{SC}} A_{\text{nw}} \frac{dT}{dx} \right) \quad (7)$$

for the normal and SC segments, respectively. For the longer wires S2 and S4, the smaller I_r values allow the short proximity region adjacent to the normal-metal pads to be neglected.

This form for the heat-removal power density per unit length assumes that phonon conduction along the wire direction is weak, a reasonable assumption since the thermal conductivity is small, and since the wire is much longer than the height of the InP ridge (i.e., $10 \mu\text{m} \gg 30 \text{ nm}$). It also assumes that the environment to which the energy is dissipated is well-anchored at the ambient temperature. For instance, if the electron-phonon relaxation is the limiting step, it is reasonable to assume that the combination of Kapitza and InP ridge phonon conduction is sufficiently large that the phonon temperature within the nanowire is maintained at T_o . On the other hand, if Kapitza boundary resistance limits the rate of heat removal via the phonons, then it is reasonable to assume the phonons within the InP ridge are at T_o .

Several choices are possible for γ . For electron-phonon energy relaxation via three-dimensional (3D) phonons, $\gamma = 5$, while for Kapitza boundary resistance $\gamma = 4$. However, the small lateral dimensions (width and/or height) in either the nanowire or InP ridge should render the phonons reduced below 3D, down to 1D and 2D, respectively. This occurs because the thermal phonon wavelength $\lambda_{\text{ph}}/2$, exceeds the lateral dimension(s) for $T \leq 1.3 \text{ K}$ [more precisely, $\lambda_{\text{ph}}/2 > (w, h)$]. Note that the width of the InP ridge is $w_{\text{InP}} = 8 \text{ nm}$ while the width/height of the nanowire w or $h \sim 10 \text{ nm}$. By examining the fitted coefficient in front of the power-law term, one seeks to exclude various possibilities. This coefficient β naturally depends on the limiting mechanism. For example, in

the case of electron-3D phonon relaxation, $\beta = \Sigma_{e\text{-3D-ph}} A_{\text{nw}}$, where $\Sigma_{e\text{-3D-ph}}$ is the 3D energy relaxation rate constant and A_{nw} the nanowire cross sectional area. For Kapitza boundary resistance limited thermal conduction with 3D InP phonons, $\beta = \sigma_{K,3\text{D-ph}} w_{\text{InP}}$, where $\sigma_{K,3\text{D-ph}} T^3$ is the Kapitza boundary conductance at temperature T .

From the quantitative analysis presented below, it will be shown that in the most likely scenario, thermal conduction is limited by the Kapitza boundary resistance between the Al nanowire and the InP ridge. Thus, it turned out not necessary to consider the inclusion of more-than-one power-law terms, each with a different exponent γ . At the same time, the assumption of a power-law form also presupposes that the conduction is dominated by intrinsic properties of nearly crystalline materials, for both the nanowire and the InP ridge, rather than by interface states or adsorbates on the side walls. A partial justification is the degree of agreement achievable with data using sensible parameter values.

These highly nonlinear equations were solved approximately by numerical methods, yielding the position dependent temperature profiles shown in Figs. 6(b) and 6(c), respectively for S2 and S4. The fitting to I_r versus temperature yielded the curves in Figs. 3(b) and 3(c), with L_o fixed at the value from wire S1, of $3.65 \times 10^{-8} \text{ W } \Omega/\text{K}^2$. The critical value x_c was found to shift slightly toward the center, to $0.23L$ [$0.46(L/2)$] rather than $L/4$ [$0.5(L/2)$]. The best fit is for $\gamma = 5$, corresponding to the electron-3D phonon energy relaxation as the limiting step. Fits of slightly lower quality can be achieved for $\gamma = 4$ or 3. On the other hand, the numerical values for the coefficient β yielded values for the parameters, which point to Kapitza boundary resistance at the Al nanowire-InP interface as the limiting path to phonon conduction.

For $\gamma = 5$ the extracted electron-3D-phonon relaxation rate $\Sigma_{e\text{-3D-ph}}$ for S2 is $\sim 6\times$ as large as the established value $\sim 2 \times 10^9 \text{ W/m}^3 \text{ K}^5$ (Ref. 18) and is $\sim 11\times$ for S4. The values are thus inconsistent. We are forced to consider the possibility that the Al phonons are reduced in dimensions down to 1D. An enhancement of $\sim \Theta_D/T(a/w) \sim 9$ can be expected per dimension reduced, where a is the lattice constant, yielding a factor ~ 81 , far larger than the measured enhancement! Instead, within this scenario, one expects the limiting step to be the Kapitza boundary resistance between the Al nanowire and the InP ridge.

For Kapitza boundary limited conduction, one may expect $\gamma = 3$ rather than $\gamma = 4$ due to reduced-dimension 2D InP phonons, despite the poorer quality fit. An enhancement factor of ~ 9 over the known 3D value should be present from the reduction in dimension by 1. As a reference, we use $\sigma_{K,3\text{D-ph}} \sim 20 \text{ W/m}^2 \text{ K}^4$, obtained for Au on GaAs rather than Al on InP.²⁵ Forcing $\gamma = 4$ yield the parameter value $\sigma_{K,3\text{D-ph}} \sim 190 \text{ W/m}^2 \text{ K}^4$, which is 10 times the reference value. Instead, after conversion of the reference value to account for 2D phonons, the enhanced value of $\sigma_{K,2\text{D-ph}} \sim 280 \text{ W/m}^2 \text{ K}^3$ is consistent with the fitted values of 300 and 330 $\text{W/m}^2 \text{ K}^3$, respectively, for S2 and S4 (with $\gamma = 3$). To make certain this picture of Kapitza boundary limited conduction is consistent, we need to ensure the ridge phonon thermal conduction is larger. An estimate of the phonon thermal conductivity of the InP ridge itself yields a lower bound of $700 \text{ W/m}^2 \text{ K}^2$,

corresponding to the case of a very short, ridge-width limited phonon mean free path ~ 8 nm. Note that in this estimate, the height of the ridge is already accounted for, and it is cast in a form to enable a direct comparison, i.e. rate of heat flow is given by $-(700 \text{ W/m}^2\text{K}^3) A T^2 \Delta T$, where A is the cross sectional area. This rules out phonon conduction in the InP ridge as the limiting step, as required. Finally, as a reference, we estimate the conductivity in the *absence* of any electronic contribution. This yield a value *roughly double* the above values for the 2D phonon Kapitza boundary conductance coefficient.

It is worthwhile to reemphasize the evidence for reduced dimension Kapitza boundary conduction as the limiting step, is based on a direct comparison of the fitting parameter values for S2 and S4. Whereas, $\Sigma_{e-3D-ph}$ (for electron-phonon-relaxation-limited heat removal) shows a discrepancy between S2 and S4 of a factor $1.2/2.2 \sim 1.8$, the values for the reduced dimension $\sigma_{K,2D-ph}$ (for 2D InP-ridge phonon, Kapitza-boundary-limited thermal conduction) are within 10% of each other! This, in conjunction with the discrepancy with the known reference value for $\Sigma_{e-3D-ph}$, helps establish the Kapitza boundary resistance limited scenario.

One factor, which may impact the quantitative agreement and account for the discrepancy between the model and the data, could come from imperfections at the nanowire-InP interface mentioned previously. For instance, grain boundaries in the polycrystalline nanowires (grain size \sim wire

width), interface roughness, localized interface states, etc., all can influence the phonon coupling across the boundary. In the ordinary 3D case between liquid He³ and a metal, it is well known that interface roughness can help break the translational invariance, and supply the momentum transfer needed to mitigate the effects of phonon velocity mismatch across the boundary. This leads to a weaker dependence than T^4 in the boundary conductance, and an enhanced conductance at low T . Unfortunately, for our nanowires such effects are difficult to quantify.

Based on the detailed analysis presented in this work, we establish that in the retrapping process, the longer wires S2 and S4 require phonons to contribute to heat removal, in addition to the electronic thermal conduction, while for the short S1, electronic conduction alone is sufficient. The reasonable fits using sensible parameters demonstrate that it is possible to achieve an understanding of the heating-induced hysteresis for nanowires S1, S2, and S4, based on heating within the normal regions, while at the same time account for the observed differences.

The research is supported by NSF DMR-0701948 (P.L., P.M.W., and A.M.C.), Department of Energy BES/MSED award No. DE-SC0002765 (Y.B., I.V.B., and G.F.), and Institute of Physics, Academia Sinica, Taipei (P.L. and A.M.C.).

*Corresponding author: yingshe@phy.duke.edu

¹N. Giordano, *Phys. Rev. Lett.* **61**, 2137 (1988).

²A. Bezryadin, C. N. Lau, and M. Tinkham, *Nature (London)* **404**, 971 (2000).

³C. N. Lau, N. Markovic, M. Bockrath, A. Bezryadin, and M. Tinkham, *Phys. Rev. Lett.* **87**, 217003 (2001).

⁴A. Rogachev, A. T. Bollinger, and A. Bezryadin, *Phys. Rev. Lett.* **94**, 017004 (2005).

⁵F. Altomare, A. M. Chang, M. R. Melloch, Y. Hong, and C. W. Tu, *Phys. Rev. Lett.* **97**, 017001 (2006).

⁶M. Tinkham, J. U. Free, C. N. Lau, and N. Markovic, *Phys. Rev. B* **68**, 134515 (2003).

⁷M. Sahu, M. H. Bae, A. Rogachev, D. Pekker, T. C. Wei, N. Shah, P. M. Goldbart, and A. Bezryadin, *Nat. Phys.* **5**, 503 (2009).

⁸P. Li, Phillip M. Wu, Yuriy Bomze, I. V. Borzenets, G. Finkelstein, and A. M. Chang, *Phys. Rev. Lett.* **107**, 137004 (2011).

⁹N. Shah, D. Pekker, and P. M. Goldbart, *Phys. Rev. Lett.* **101**, 207001 (2008).

¹⁰W. A. Little, *Phys. Rev.* **156**, 396 (1967).

¹¹J. S. Langer and V. Ambegaokar, *Phys. Rev.* **164**, 498 (1967).

¹²D. E. McCumber and B. I. Halperin, *Phys. Rev. B* **1**, 1054 (1970).

¹³A. D. Zaikin, D. S. Golubev, A. van Otterlo, and G. T. Zimányi, *Phys. Rev. Lett.* **78**, 1552 (1997).

¹⁴D. S. Golubev and A. D. Zaikin, *Phys. Rev. B* **64**, 014504 (2001).

¹⁵S. Khlebnikov, and L. P. Pryadko, *Phys. Rev. Lett.* **95**, 107007 (2005).

¹⁶J. E. Mooij and Y. V. Nazarov, *Nat. Phys.* **2**, 169 (2006).

¹⁷J. E. Mooij and C. J. P. M. Harmans, *New J. Phys.* **7**, 219 (2005).

¹⁸H. Courtois, M. Meschke, J. T. Peltonen, and J. P. Pekola, *Phys. Rev. Lett.* **101**, 067002 (2008).

¹⁹M. Tinkham, *Introduction to Superconductivity*, International Series in Pure and Applied Physics, 2nd ed. (McGraw Hill, New York, 1996).

²⁰F. Altomare, A. M. Chang, M. R. Melloch, Y. Hong, and C. W. Tu, *Appl. Phys. Lett.* **86**, 172501 (2005).

²¹M. H. Devoret, J. M. Martinis, and J. Clarke, *Phys. Rev. Lett.* **55**, 1908 (1985).

²²V. M. Krasnov, T. Bauch, S. Intiso, E. Hürfeld, T. Akazaki, H. Takayanagi, and P. Delsing, *Phys. Rev. Lett.* **95**, 157002 (2005).

²³J. M. Kivioja, T. E. Nieminen, J. Claudon, O. Buisson, F. W. J. Hekking, and J. P. Pekola, *Phys. Rev. Lett.* **94**, 247002 (2005).

²⁴G. R. Boogaard, A. H. Verbruggen, W. Belzig, and T. M. Klapwijk, *Phys. Rev. B* **69**, 220503 (2004).

²⁵P. Mohanty, D. A. Harrington, K. L. Ekinci, Y. T. Yang, M. J. Murphy, and M. L. Roukes, *Phys. Rev. B* **66**, 085416 (2002).